



RESEARCH LETTER

10.1002/2014GL061115

Key Points:

- High-resolution lithospheric images are retrieved by a two-step joint inversion
- Three-dimensional geometry of the east subducting slab under Taiwan is established
- A possible slab deflection is observed at around latitude 23.2°N

Supporting Information:

- Figure S1
- Figure S2
- Figure S3
- Figure S4
- Text S1

Correspondence to:

H.-H. Huang,
hhhuang@earth.sinica.edu.tw

Citation:

Huang, H.-H., Y.-M. Wu, X. Song, C.-H. Chang, H. Kuo-Chen, and S.-J. Lee (2014), Investigating the lithospheric velocity structures beneath the Taiwan region by nonlinear joint inversion of local and teleseismic *P* wave data: Slab continuity and deflection, *Geophys. Res. Lett.*, 41, 6350–6357, doi:10.1002/2014GL061115.

Received 4 JUL 2014

Accepted 26 AUG 2014

Accepted article online 28 AUG 2014

Published online 18 SEP 2014

Investigating the lithospheric velocity structures beneath the Taiwan region by nonlinear joint inversion of local and teleseismic *P* wave data: Slab continuity and deflection

Hsin-Hua Huang¹, Yih-Min Wu², Xiaodong Song³, Chien-Hsin Chang⁴, Hao Kuo-Chen⁵, and Shiann-Jong Lee¹

¹Institute of Earth Sciences, Academia Sinica, Taipei, Taiwan, ²Department of Geosciences, National Taiwan University, Taipei, Taiwan, ³Department of Geology, University of Illinois at Urbana-Champaign, Urbana, Illinois, USA, ⁴Central Weather Bureau, Taipei, Taiwan, ⁵Institute of Geophysics, National Central University, Jhongli, Taiwan

Abstract The interaction between two flipping subduction systems shapes the complicated lithospheric structures and dynamics around the Taiwan region. Whether and in what form the Eurasian Plate subducts/deforms under Taiwan Island is critical to the debate of tectonic models. Although an east dipping high-velocity anomaly down to a depth below 200 km has been reported previously, its detailed morphology remains uncertain and leads to different interpretations. With a two-step strategy of nonlinear joint inversion, the slab images of the Eurasian Plate were retrieved in a geometry that is hyperthin in the south, becoming massive and steeper in the central, and severely deformed in the north. The possible depth and dimension of a slab break were also investigated through synthetic tests of whether the slab had torn. Moreover, the slab deflection found at ~23.2°N latitude seems to correspond to where the nonvolcanic tremors and recent NW-SE striking structures have occurred in southern Taiwan.

1. Introduction

The Taiwan orogeny created by the convergence between the Eurasian Plate (EP) and the Philippine Sea Plate (PSP) is intricately bracketed by two suborthogonal subduction systems (Figure 1a). The PSP to the east is subducting northward to the EP along the Ryukyu trench, whereas to the south, the EP is subducting under the PSP eastward at the Manila trench, creating a distinct subduction flipping system. Although the morphology of the PSP and the EP offshore along the trenches can be identified in local tomography studies [Wu *et al.*, 2009a, 2009b; Huang *et al.*, 2014] and by the Wadati-Benioff zones, the morphology between the two trenches under Taiwan Island has remained enigmatic. Whether and in what form the EP subducts/deforms under Taiwan Island is therefore critical to various tectonic models of Taiwan [e.g., Suppe, 1981, 1984; Wu *et al.*, 1997; Shyu *et al.*, 2005]. The thin-skin [Suppe, 1981] and thick-skin models [Wu *et al.*, 1997], for instance, require the subduction and nonsubduction of the EP, respectively. In the case of EP subduction, a break of the entire slab or crustal component is proposed to account for the mechanism of subduction flipping [Teng *et al.*, 2000; Lallemand *et al.*, 2001] and crustal exhumation [Lin, 2002]. The tandem suturing model [Lu and Hsu, 1992; Shyu *et al.*, 2005], in contrast, suggested the subduction of South China Sea plate under Taiwan.

Due to the abrupt vanishing of subduction events north of latitude 23°N, the resolution of the local earthquake tomography is restricted to a shallow depth of approximately 40 km in central Taiwan, with almost no imaging capability of the deeper structure, e.g., the subducting slab. The observations from teleseismic relative traveltimes [Chen *et al.*, 2004] and slab-induced refracted phases [Lin, 2009] suggested the presence of an aseismic subducting slab under central Taiwan, although it is difficult to constrain its geometry and dimension. Wang *et al.* [2006, 2009] and Kuo-Chen *et al.* [2012] extended the resolution of tomographic imaging to a deeper depth by incorporating teleseismic data, and both found an east dipping anomaly of high *P* wave velocity (*V_p*) continuously to the depth of at least 200 km. The former interpreted this anomaly as the subducting EP, whereas the latter proposed the possibility of continental eclogitization due to the collision-induced thickening process. Thus, the role that the EP plays under the Taiwan Island is still not well understood. To investigate the 3-D geometry of the EP in more detail, two recent large local data sets [Kuo-Chen *et al.*, 2012; Huang *et al.*, 2014] and the teleseismic data measured in this study were collected

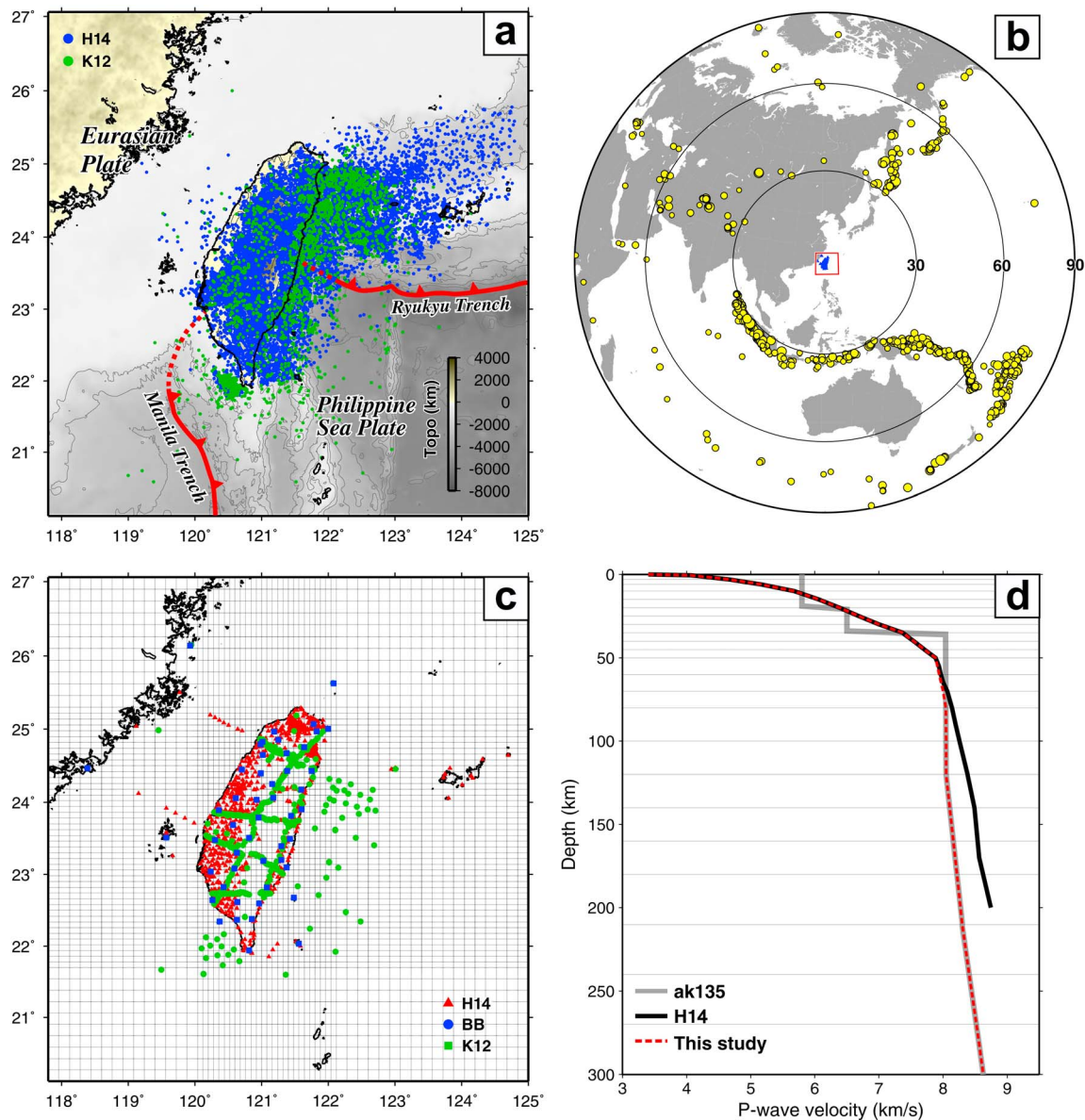


Figure 1. (a) Tectonic map with the distribution of local earthquakes from the K12 [Kuo-Chen *et al.*, 2012] and H14 [Huang *et al.*, 2014] models. The topography/bathymetry is colored in the background. (b) The distribution of teleseismic events recorded by the broadband seismic network of Taiwan (blue triangles). The red box denotes the study area for the tomographic inversion. (c) The combined station map superimposed on the model grids. We used a flexible-gridding model parameterization with finer-grid spacing around the island and with coarser spacing for far-shore areas according to the event-station coverage. [Thurber and Eberhart-Phillips, 1999] (d) The 1-D initial model of *P* wave velocity (*V_p*) derived from the 3-D averaged local model (H14) [Huang *et al.*, 2014] and the 1-D global model *ak135* [Kennett *et al.*, 1995] for shallow- and deep-velocity structures, respectively. The layers show the vertical parameterization of our model with an increasing interval in depth.

for a two-step joint inversion (Figure 1). A prominent geometrical variation of the EP was imaged and verified through various synthetic tests. The resolved slab images exhibit distinct characteristics from south to north, providing a constraint on the tectonic process of Taiwan orogeny. Based on the tomographic observations, we constructed a schematic 3-D slab model of the EP and suggest an ongoing continental subduction of the EP as evidenced by the continuity and the thickness of the slab images.

2. Data Reinforcement and Inversion Strategy

To demonstrate the complementarity of each of the two local data sets from the studies of Kuo-Chen *et al.* [2012] and Huang *et al.* [2014], we assessed their different advantages in the data and the station

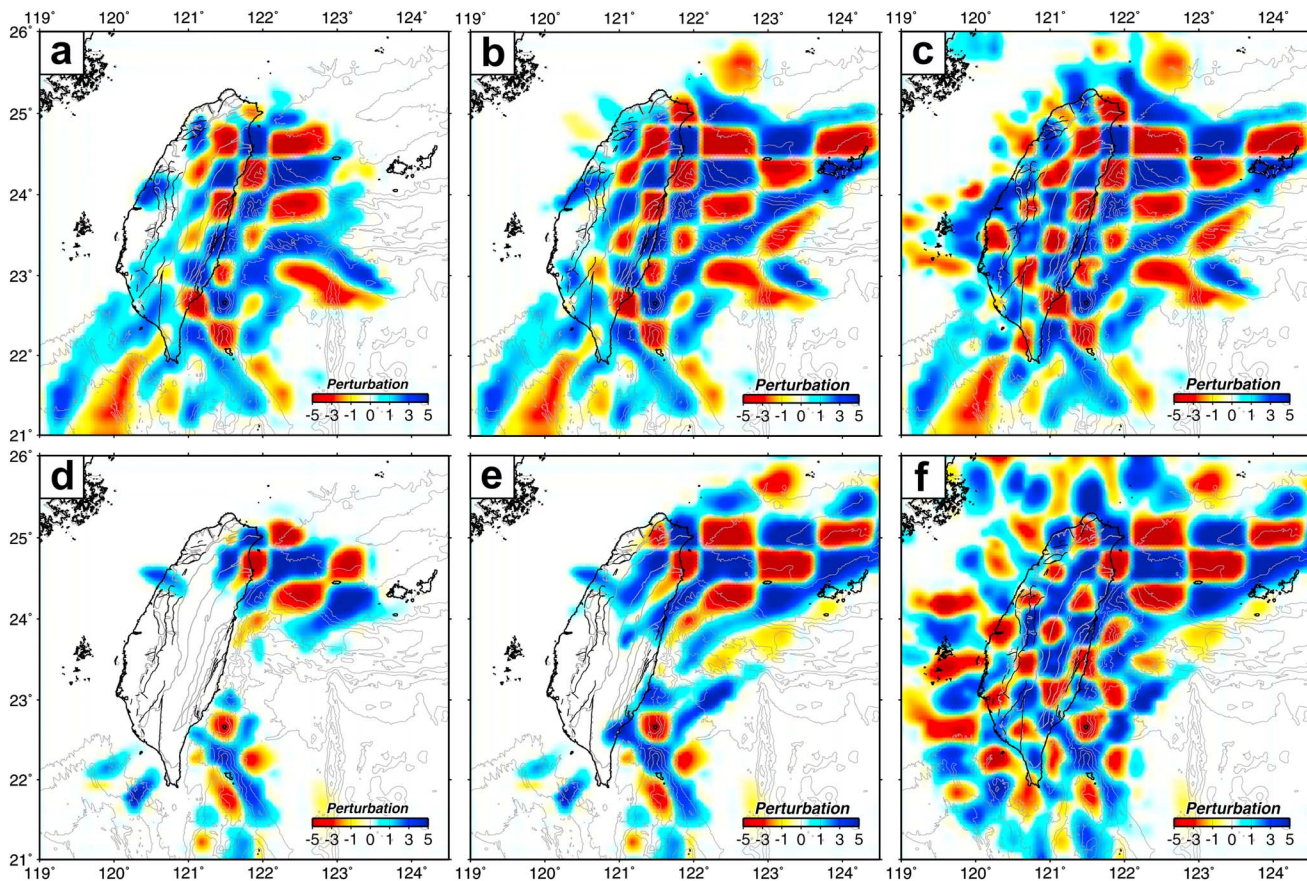


Figure 2. Recovered images in checkerboard tests at depths of (a–c) 60 and (d–f) 100 km for different data sets. From left to right, we verified the resolution coverage for the data from K12 only (Figures 2a and 2d), K12 + H14 (Figures 2b and 2e), and K12 + H14 + teleseismic events (Figures 2c and 2f) sequentially.

coverage through checkerboard tests (Figures 2a, 2b, 2d, and 2e). The models obtained from each data set are termed K12 and H14, respectively, hereafter. In Figure 2, the recovered image obtained solely from the data set of *Kuo-Chen et al.* [2012] shows broad resolution to the far eastern offshore region due to the deployment of ocean bottom seismometers (Figure 1c). In contrast, adding the data set of *Huang et al.* [2014], which has a much longer data recording period and includes the Japanese stations on the Ryukyu Arc, can further reinforce the resolution at deeper depths and in northern Taiwan for the PSP subduction. This difference is clearly demonstrated in the images at the depth of 100 km (Figures 2d and 2e). Combining these two local data sets, a total of 1716 stations, 9962 events, and 111,957 *P* wave readings were used.

In addition to local data, we further collected 1550 teleseismic events in a distance range of 30°–90° worldwide recorded by the island-wide broadband network of 49 stations (Figures 1b and 1c). This broadband network is composed of two arrays which are operated by the Central Weather Bureau and the Institute of Earth Sciences, Academia Sinica (IES), respectively. The one operated by IES is affiliated with the program of Broadband Array in Taiwan for Seismology. To obtain a reliable teleseismic relative arrival time in the vertical component of a *P* wave, we first utilized the *TauP* toolkit [Crotwell et al., 1999] to predict the theoretical arrival of a *P* wave with a global 1-D model, *ak135* [Kennett et al., 1995], and cut a relatively longer time window of 60 s to ensure the inclusion of the real arrival time. Then, an autopicking algorithm [Earle and Shearer, 1994] was adopted to identify the accurate arrival time within the 60 s time window with a threshold of $STA/LTA = 5$ (short-term average to long-term average ratio). If this arrival time was found, we further cut a shorter time window of 15 s for waveform cross correlation in a frequency band of 0.02–0.2 Hz. This procedure ensures that the real energetic *P* wave arrivals are found and are cross-correlated in a short time window excluding the noise or other irrelevant phases. After the cross-correlations of all stations to one event as acquired, a least squares method [VanDecar and Crosson, 1990] was used to

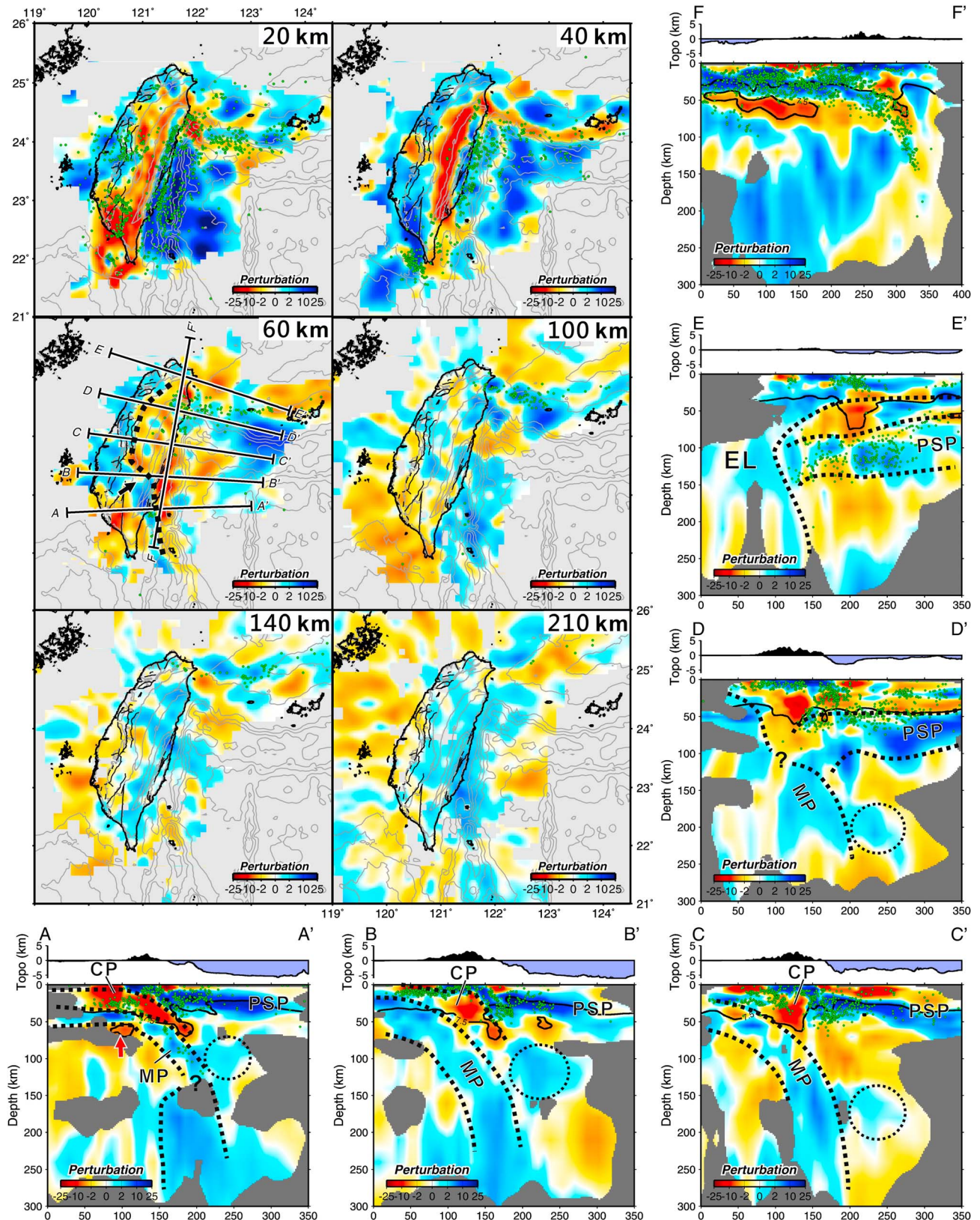


Figure 3

calculate the teleseismic relative arrival times. As a result, 19,083 relative times for the teleseismic events were obtained by this procedure with double check using visual inspection.

The teleseismic tomography was first introduced by *Aki et al.* [1977] and later developed to integrate local earthquakes into a joint inversion scheme [*Roecker et al.*, 1993; *Zhao et al.*, 1994] for gaining higher-resolution images of the crust-to-upper mantle velocity structures in a specific local region, compared with those in the global tomography [*Bijwaard et al.*, 1998; *Li et al.*, 2008]. To eliminate the path effect outside the local target model and to incorporate with local seismic data, the teleseismic data are used in a

demeaned form as $\tilde{r}_i^j = r_i^j - \frac{1}{n} \sum_{j=1}^{n_s} r_i^j$, where r_i^j and \tilde{r}_i^j represent the absolute and demeaned relative

traveltime residuals, respectively. The merit of working with teleseismic data is clearly illustrated in Figures 2c and 2f. Combining the teleseismic data fills the resolution gap of local earthquake tomography under central Taiwan and also expands the lateral resolution westward to cover the entire island area at depth. This capability is particularly important for this study to investigate the lithospheric structures under the Taiwan Island.

As the ray density of a teleseismic data set is usually lower than that of a local data set, a joint inversion often suffers the problem of model parameterization to optimize the use of both data sets. To focus on deep lithospheric structures, it often degrades the gridding space of the model (either in the horizontal or vertical direction) to accommodate the lower and sparser ray distribution of teleseismic data, with a sacrifice of the higher resolution at shallow depths by local data [*Wang et al.*, 2006, 2009; *Kuo-Chen et al.*, 2012]. Teleseismic imaging, however, is seriously biased by crustal heterogeneity, in particular, for a highly heterogeneous area such as Taiwan, we argue that it could be quite difficult to retrieve high-resolution lithospheric velocity structures without taking into account accurate crustal structures as much as possible. Thus, rather than determining two scales of models as in *Kuo-Chen et al.* [2012], a two-step strategy is adopted for the joint inversion in the present study. The model is parameterized in a flexible gridding with finer-grid spacing around the Island and with coarser spacing for far-shore areas to account for event-station distributions of local and teleseismic data sets (Figure 1c). The initial 1-D model was derived by combining the 1-D average of previous 3-D model in the shallow depth [*Huang et al.*, 2014] and the global 1-D model *ak135* for the deep depth [*Kennett et al.*, 1995] (Figure 1d). Using the local data only, we first implemented a local tomographic inversion where mostly covered by finer gridding over the island for high-resolution crustal structures. Then the joint inversion of local and teleseismic data was conducted with the obtained 3-D local model as the initial model. For the traveltime calculation, we used the modified pseudobending method in a 3-D spherical coordination [*Um and Thurber*, 1987; *Koketsu and Sekine*, 1998; *Sun and Song*, 2008; *Xu and Song*, 2010] and retraced the teleseismic rays iteratively, as done for the local earthquake tomography, in a fully nonlinear manner without fixing the incident points of teleseismic rays at the bottom of the model. For a demonstration of the nonlinear effect, please refer to section S1 in the supporting information.

3. Tomographic Images and Verification

The two-step inversion reduced the total residual root-mean-square significantly from 0.52 to 0.16 s (approximately 69%) after 10 iterations (five for local data only and five for all data including teleseismic events). Through the stepwise process, we are able to retain most of the detailed crustal structures in the model while accounting more accurately for the teleseismic data (horizontal slices at 20 and 40 km in Figure 3). At 20 km depth in particular, the shape of high Vp along western coast is well correlated with the geometry of the preorogeny continental margin [*Lin et al.*, 2003]. The combination of the K12 and H14 data sets also shows its strength in enhancing the imaging of both the south and the east subduction (horizontal slices at 40 and 60 km). Below the depth of 60 km, the effect of using the teleseismic data starts to appear in the images. The N-S trending, east dipping EP can be readily identified throughout the depths. The

Figure 3. Tomographic images of horizontal slices and vertical profiles. The locations of the profiles in map view are shown in the slice of 60 km depth. The possible slab deflection is indicated by the black arrow. In the profiles, the black solid line is the $V_p = 7.5$ km/s contour of the reference of the Moho interface. Relocated earthquakes are denoted by green dots. Poorly resolved areas are blanked (in dark gray) by the index of resolvability, R , converted from the checkerboard test results [*Huang et al.*, 2013, 2014]. Dashed lines are the outlines of the structures we interpreted. PSP, Philippine Sea Plate; EL, Eurasian lithosphere; CP, the crustal part of the subducting slab; and MP, the mantle part of the subducting slab. The red arrow indicates the low- V_p anomaly likely related to the ancient rifting event. The high- V_p anomaly consistently observed is denoted by the dotted circle.

other prominent feature revealed in the horizontal slices is a NW-SE trending deflection of the slab around latitude 23.2°N at the depth of 60 km, which can be shown more clearly in the profile AA' to CC' with a retreat of Moho interface to the west (top of MP denoted by dotted line). To the south, the high-Vp slab image is narrow and striking NNW-SSE, whereas to the north, the slab turns nearly N-S and becomes wider. The subducting PSP to the east of Taiwan is well imaged throughout the slices, in close agreement with the subduction events (green dots). In vertical profiles, the black solid line represents the $V_p = 7.5$ km/s contour as the reference of the Moho interface. Low-resolution areas in the images are blanked (in dark gray) by the resolvability index converted from the checkerboard test results [Huang *et al.*, 2013, 2014]. From the southernmost Profile AA', a hyperthin slab-like anomaly of high Vp overlain by a thick layer of low Vp is observed, which is the narrow Vp zone to the south of the deflection that we observed in the slice at the 60 km depth. Northward across the deflection, in Profiles BB' and CC', a massive and steeper high-Vp zone is present instead, indicating that the eastward subduction could be down to more than 200 km deep. Given the Moho reference ($V_p = 7.5$ km/s), the accretionary prism changes its shape from a singly vergent to a doubly vergent wedge (Profile AA'–CC'), indicating the gradual influence from PSP in the east. In Profile DD', which is the most intriguing one, the high-Vp zone shows a break (approximately 100 km in horizontal distance) in the east dipping continuity but is more likely connected with the west dipping zone to the east. However, when further compared with Profile EE', it is clear that the west dipping zone with a strong amplitude in Profile DD' is a transection of the northward subducting PSP (or its mantle component). Therefore, the high-Vp slab signal in the DD' profile is more likely still dipping east with a retreat of the shallow portion (above the 100 km depth) due to the westward impingement of the PSP, showing strong deformation of collision. The subducting PSP is then carving and blocked by the Eurasian lithosphere to the west in the EE' profile, and the strong low-Vp anomaly immediately above it implies the melting activities beneath the Okinawa Trough. The Profile FF' along the westernmost PSP, which is roughly perpendicular to all E-W profiles, displays another view of the 3-D east dipping slab anomaly under the Taiwan Island. The relatively thin subhorizontal high-Vp zone on the left of the horizontal distance at approximately 80 km is related to the hyperthin slab observed in the AA' profile. On the right of the horizontal distance at 80 km (corresponding to Profile BB'–DD'), the high-Vp zone becomes much more massive and steeper (i.e., thicker when cut along the N-S strike) and seems blurred and diminished as the PSP crosses at the horizontal distance of approximately 280 km. This pattern also indicates that the subduction of the EP may not extend to the north of the junction with the PSP; however, due to the high complexity in this region (3-D slab interaction, postcollision mountain collapse, the Ryukyu back-arc system, volcanic magmatism), more data are needed to draw firm conclusions.

We carefully verified the images through various synthetic tests with different synthetic slab models (Figures S2–S4). The results show that a continuous slab model is more easily recovered than the slab break model due to the nature of the relatively poor vertical resolution of teleseismic data and the short aperture of the on-land broadband stations. By testing different gap sizes of the slab break, we conclude that the joint inversion model cannot distinguish a gap of 40 km but can distinguish a gap of greater than 80 km (Figure S4). These findings may show the limitation of the tomographic technique to some extent but also could provide important insights into the tectonic interpretations described in the following section.

4. Tectonic Implications and Discussion

A 3-D schematic slab model was established based on tomographic observations (Figure 4). In the south (Profile AA'), as the thick low-Vp layer sitting atop the high-Vp slab likely represents the continental crust being partially pulled down to a depth of about 80 km, which is also observed elsewhere in the Pamir [Sippl *et al.*, 2013] and Greece [Pearce *et al.*, 2012], the hyperthin high-Vp anomaly is better interpreted as a hyperrifted mantle of the continental plate rather than a relatively thin oceanic plate (e.g., South China Sea Plate). Recently, using seismic reflection and wide-angle data, McIntosh *et al.* [2013] found a hyperextended crust in southernmost Taiwan and related it with an ancient failed rift event. If their conclusion is true, the failed rift would have also eroded/extended the mantle of the plate, as observed in the AA' profile. Northward across the deflection at the latitude of $\sim 23.2^{\circ}\text{N}$ (Profile BB' and CC'), the east dipping slab image turns steeper and massive, showing a normal thickness of continental mantle. The crust seems thicker and less subducting with the slab. Further to the north (Profile DD'), the shallow portion of the mantle then starts retreating due to the westward impingement of the PSP (denoted by dotted line). In fact, previous

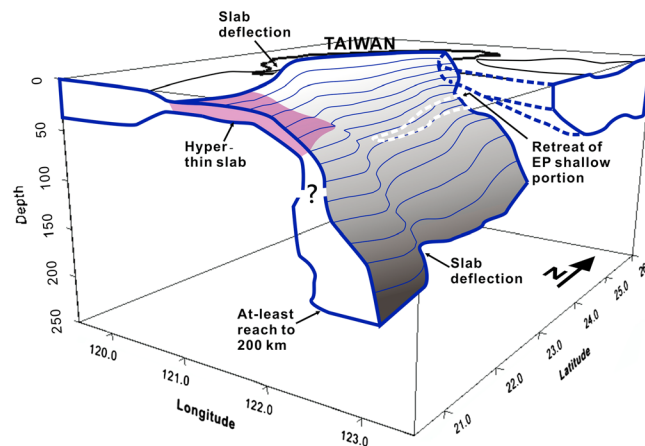


Figure 4. The 3-D schematic model of the Eurasian Plate beneath the Taiwan region. The slab geometry and thickness are based on the tomographic images (Figure 3) to the first order showing the hyperthin slab (shaded zone) related to ancient failed rift event and the NW-SE trending deflection around the latitude of 23.2°N.

studies of regional [Koulakov *et al.*, 2014] and global tomography [Lallemant *et al.*, 2001; Li *et al.*, 2008] have confirmed the presence of a massive high-Vp slab at great depth under Taiwan but lacked a good resolution at shallow depth. The building of the detailed 3-D geometry of the EP in this study could therefore bridge the gap for studying the tectonics of this region.

Another scenario we cannot exclude thus far is that the EP may have already torn/broken in some places instead of being an intact continuous plate. However, according to the slab break tests, we can restrict the tear dimension to less than 80 km and the location most likely within a depth range of approximately 100–150 km; at

depths outside this range, the tear does not appear to exist. This result implies that the extensive slab tearing may not have occurred yet. Whether such an 80 km size tear can accommodate the flipping of the subduction then becomes an extended question [Teng *et al.*, 2000; Lallemant *et al.*, 2001]. Slab breaking may also change the mantle flow distinctly. Therefore, geodynamic modeling and shear wave splitting studies may help with further verification of this possibility.

In addition, a few features of the tomographic images seem meaningful but have yet been elucidated. The NW-SE trending slab deflection around latitude 23.2°N, for example, is a feature that spatially coincides with the location and the strike of the Jiasian earthquake sequence [Huang *et al.*, 2011] as well as the location of the tremor/swarm sources in southern Taiwan [Peng and Chao, 2008; Chuang *et al.*, 2014]. The NW-SE trending sequence of the Jiasian earthquake (different from the NE-SW trending of the Taiwan orogeny) and the tremor/swarm activity observed in southern Taiwan at deep depths still lack explicit mechanisms. We speculate that this deflection may serve the mechanism prompting the local disturbance of stress state and deep dehydration process, even though further analyses will be required. Moreover, there is a consistent high-Vp anomaly appearing through Profile AA'–DD' (enclosed by the dotted circle). It can also be found commonly in the profiles of previous studies at similar locations [Wang *et al.*, 2009; Kuo-Chen *et al.*, 2012] and therefore may not be an artifact due to inversion and present used data set. This anomaly could represent a remnant structure of earlier subduction episode or the eclogitized subducted continental crust as it appears at the ends of continuous low-Vp zones [Sippl *et al.*, 2013]. However, the latter should trigger the occurrence of intermediate depth earthquakes, due to the dehydration embrittlement [Hacker *et al.*, 2003], which have not been observed under central Taiwan.

The interaction between multiple subduction systems, such as Indonesia-Tonga [e.g., Hall and Spakman, 2002], Izu-Bonin-Mariana [e.g., Miller *et al.*, 2005], and central Mediterranean regions [e.g., Giacomuzzi *et al.*, 2012], often results in complicated slab structures. At the Ryukyu-Manila trench junction of Taiwan (with flipping subductions), our images demonstrated how a massive continental plate (EP) can deform and vary greatly in geometry with a relatively thin oceanic plate (PSP) at small distance. Better understanding of such interaction morphology is important to illuminate the complexity of regional tectonics between plates and associated orogeny.

References

- Aki, K., A. Christofferson, and E. S. Husebye (1977), Determination of the three-dimensional seismic structure of the lithosphere, *J. Geophys. Res.*, **82**, 277–296, doi:10.1029/JB082i002p00277.
- Bijwaard, H., W. Spakman, and E. R. Engdahl (1998), Closing the gap between regional and global travel time tomography, *J. Geophys. Res.*, **103**, 30,055–30,078, doi:10.1029/98JB02467.
- Chen, P. F., B. S. Huang, and W. T. Liang (2004), Evidence of a slab of subducted lithosphere beneath central Taiwan from seismic waveforms and travel times, *Earth Planet. Sci. Lett.*, **229**, 61–71.

Acknowledgments

We thank the Central Weather Bureau (<http://gdms.cwb.gov.tw/index.php>), the Broadband Array in Taiwan for Seismology (<http://tecws.earth.sinica.edu.tw/BATS/>), the Taiwan Integrated Geodynamics Research project, Nation Central University, and the Taiwan Ocean Research Institute for providing the seismic data for this integrated work. We thank Timothy Byrne and Steven Roecker, who improved and refined the manuscript. We are also grateful for the valuable discussion with John Suppe, Shu-Huei Hung, Li Zhao, J. Bruce H. Shyu, Wen-Shan Chen, and Ban-Yuan Kuo. This work is supported by Ministry of Science and Technology, Taiwan.

The Editor thanks Timothy Byrne and Steven Roecker for their assistance in evaluating this paper.

- Chuang, L. Y., K. H. Chen, A. Wech, T. Byrne, and W. Peng (2014), Ambient tremors in a collisional orogenic belt, *Geophys. Res. Lett.*, *41*, 1485–1491, doi:10.1002/2014GL059476.
- Crotwell, H. P., T. J. Owens, and J. Ritsema (1999), The TauP toolkit: Flexible seismic travel-time and ray-path utilities, *Seismol. Res. Lett.*, *70*(2), 154–160.
- Earle, P. S., and P. M. Shearer (1994), Characterization of global seismograms using an automatic-picking algorithm, *Bull. Seismol. Soc. Am.*, *84*(2), 366–376.
- Giacomuzzi, G., M. Civalleri, P. De Gori, and C. Chirabba (2012), A 3D Vs model of the upper mantle beneath Italy: Insight on the geodynamics of central Mediterranean, *Earth Planet. Sci. Lett.*, *335–336*, 105–120.
- Hacker, B., S. Peacock, G. Abers, and S. G. Holloway (2003), Subduction factory 2. Are intermediate-depth earthquakes in subducting slabs linked to metamorphic dehydration reactions?, *J. Geophys. Res.*, *108*(B1), 2030, doi:10.1029/2001JB001129.
- Hall, R., and W. Spakman (2002), Subducted slabs beneath the eastern Idoesia-Tonga region: Insights from tomography, *Earth Planet. Sci. Lett.*, *201*(2), 321–336.
- Huang, H. H., Y. M. Wu, T. L. Lin, W. A. Chao, J. B. H. Shyu, C. H. Chan, and C. H. Chang (2011), The preliminary study of the 4 March 2010 Mw6.3 Jiasian, Taiwan, earthquake sequence, *Terres. Atmos. Oceanic Sci.*, *22*(3), 283–290.
- Huang, H. H., Z. J. Xu, Y. M. Wu, X. Song, B. S. Huang, and N. L. Minh (2013), First local seismic tomography for Red River shear zone, northern Vietnam: Stepwise inversion employing crustal P and Pn waves, *Tectonophysics*, *584*, 230–239.
- Huang, H. H., Y. M. Wu, X. Song, C. H. Chang, S. J. Lee, T. M. Chang, and H. H. Hsieh (2014), Joint Vp and Vs tomography of Taiwan: Implications for subduction-collision orogeny, *Earth Planet. Sci. Lett.*, *392*, 177–191.
- Kennett, B. L. N., E. R. Engdahl, and R. Buland (1995), Constraints on seismic velocities in the Earth from travel times, *Geophys. J. Int.*, *122*, 108–112.
- Koketsu, K., and S. Sekine (1998), Pseudo-bending method for three-dimensional seismic ray tracing in a spherical earth with discontinuities, *Geophys. J. Int.*, *132*, 339–346.
- Koulakov, I., Y. M. Wu, H. H. Huang, N. Dobretsov, A. Jakovlev, I. Zabelina, K. Jaxybulatov, and V. Chervov (2014), Slab interactions in the Taiwan region based on the P- and S-velocity distributions in the upper mantle, *J. Asian Earth Sci.*, *79*, 53–64.
- Kuo-Chen, H., F. T. Wu, and S. W. Roecker (2012), Three-dimensional P velocity structures of the lithosphere beneath Taiwan from the analysis of TAIGER and related seismic data sets, *J. Geophys. Res.*, *117*, B06306, doi:10.1029/2011JB009108.
- Lallemand, S., Y. Font, H. Bijwaard, and H. Kao (2001), New insights on 3-D plates interaction near Taiwan from tomography and tectonic implications, *Tectonophysics*, *335*, 229–253.
- Li, C., R. D. van der Hilst, E. R. Engdahl, and S. Burdick (2008), A new global model for P wave speed variations in Earth's mantle, *Geochem. Geophys. Geosyst.*, *9*, Q05018, doi:10.1029/2007GC001806.
- Lin, A. T., A. B. Watts, and S. P. Hesselbo (2003), Cenozoic stratigraphy and subsidence history of the South China Seamargin in the Taiwan region, *Basin Res.*, doi:10.1046/j.1365-2117.2003.00215.x.
- Lin, C. H. (2002), Active continental subduction and crustal exhumation: The Taiwan orogeny, *Terra Nova*, *14*, 281–287.
- Lin, C. H. (2009), Compelling evidence of an aseismic slab beneath central Taiwan from a dense linear seismic array, *Tectonophysics*, *466*, 205–212.
- Lu, C. Y., and K. J. Hsu (1992), Tectonic evolution of the Taiwan mountain belt, *Petrol. Geol. Taiwan*, *27*, 21–46.
- McIntosh, K., H. van Avendonk, L. Lavier, W. R. Lester, D. Eakin, F. T. Wu, C. S. Liu, and C. S. Lee (2013), Inversion of a hyper-extended rifted margin in the southern Central Range of Taiwan, *Geology*, doi:10.1130/G34402.1.
- Miller, M. S., A. Gorbato, and B. L. N. Kennett (2005), Heterogeneity within the subducting Pacific slab beneath the Izu-Bonin-Mariana arc: Evidence from tomography using 3D ray tracing inversion techniques, *Earth Planet. Sci. Lett.*, *235*, 331–342.
- Pearce, F. D., S. Rondenay, M. Sachpazi, M. Charalampakis, and L. H. Royden (2012), Seismic investigation of the transition from continental to oceanic subduction along the western Hellenic subduction zone, *J. Geophys. Res.*, *117*, B07306, doi:10.1029/2011JB009023.
- Peng, Z., and K. Chao (2008), Non-volcanic tremor beneath the Central Range in Taiwan triggered by the 2001 Mw 7.8 Kunlun earthquake, *Geophys. J. Int.*, doi:10.1111/j.1365-246X.2008.03886.x.
- Roecker, S. W., T. M. Sabitova, L. P. Vinnik, Y. A. Burmakov, M. I. Golvanov, R. Mamatkanova, and L. Munirova (1993), Three-dimensional elastic wave velocity structure of the western and central Tien Shan, *J. Geophys. Res.*, *98*(B9), 15,779–15,795, doi:10.1029/93JB01560.
- Shyu, J. B. H., K. Sieh, and Y. G. Chen (2005), Tandem suturing and disarticulation of the Taiwan orogen revealed by its neotectonic elements, *Earth Planet. Sci. Lett.*, *233*, 167–177.
- Sippl, C., et al. (2013), Deep burial of Asian continental crust beneath the Pamir imaged with local earthquake tomography, *Earth Planet. Sci. Lett.*, *384*, 165–177.
- Sun, X. L., and X. D. Song (2008), Tomographic inversion for three-dimensional anisotropy of Earth's inner core, *Phys. Earth Planet. Inter.*, *167*, 53–70, doi:10.1016/j.pepi.2008.02.011.
- Suppe, J. (1981), Mechanics of mountain building and metamorphism in Taiwan, *Mem. Geol. Soc. China*, *4*, 67–89.
- Suppe, J. (1984), Kinematics of arc-continent collision, flipping of subduction, and back-arc spreading near Taiwan, *Mem. Geol. Soc. China*, *6*, 21–33.
- Teng, L. S., C. T. Lee, Y. B. Tsai, and L. Y. Hsiao (2000), Slab breakoff as a mechanism for flipping of subduction polarity in Taiwan, *Geology*, *28*, 155–158.
- Thurber, C., and D. Eberhart-Phillips (1999), Local earthquake tomography with flexible gridding, *Comput. Geosci.*, *25*, 809–818.
- Um, J., and C. Thurber (1987), A fast algorithm for two-point seismic ray tracing, *Bull. Seismol. Soc. Am.*, *77*, 972–986.
- VanDecar, J. C., and R. S. Crosson (1990), Determination of teleseismic relative phase arrival times using multi-channel cross-correlation and least squares, *Bull. Seism. Soc. Am.*, *80*(1), 150–169.
- Wang, Z., D. Zhao, J. Wang, and H. Kao (2006), Tomographic evidence for the Eurasian lithosphere subducting beneath south Taiwan, *Geophys. Res. Lett.*, *33*, L18306, doi:10.1029/2006GL027166.
- Wang, Z., Y. Fukao, D. Zhao, S. Kodaira, O. P. Mishra, and A. Yamada (2009), Structural heterogeneities in the crust and upper mantle beneath Taiwan, *Tectonophysics*, *476*, 460–477, doi:10.1016/j.tecto.2009.07.018.
- Wu, F. T., R. J. Rau, and D. Salzberg (1997), Taiwan orogeny: Thin-skinned or lithospheric collision?, *Tectonophysics*, *274*, 191–220.
- Wu, Y. M., J. B. H. Shyu, C. H. Chang, L. Zhao, M. Nakamura, and S. K. Hsu (2009a), Improved seismic tomography offshore northeastern Taiwan: Implications for subduction and collision processes between Taiwan and the southernmost Ryukyu, *Geophys. J. Int.*, *178*, 1042–1054.
- Wu, Y. M., C. H. Chang, L. Zhao, N. C. Hsiao, Y. G. Chen, and S. K. Hsu (2009b), Relocation of the 2006 Pingtung earthquake sequence and seismotectonics in southern Taiwan, *Tectonophysics*, *479*, 19–27, doi:10.1016/j.tecto.2008.12.001.
- Xu, Z. J., and X. D. Song (2010), Joint inversion for crustal and Pn velocities and Moho depth for eastern margin of Tibetan Plateau, *Tectonophysics*, *491*, 185–193.
- Zhao, D., A. Hasegawa, and H. Kanamori (1994), Deep structure of Japan subduction zone as derived from local, regional, and teleseismic events, *J. Geophys. Res.*, *99*(B11), 22,313–22,329, doi:10.1029/94JB01149.